Universidad de La Laguna

Facultad de Ciencias

Initiation to the methods of theoretical study of materials.

Degree Final Project

Author:

Dácil Idaira Yánez Martín

Supervised by:
Dr. Andrés Mújica Fernaud
Dra. Silvana Radescu Cioranescu

Academic Year 2020/2021

Contents

Acknowledgements

Abstract

En este trabajo se ha realizado un estudio general de la Teoría del Funcional Densidad (DFT por sus siglas en ingles), en el cual nos hemos centrado en la demostración de los teoremas que fundamentan la base de esta teoría. Haciendo uso del programa VASP, el cual implementa la DFT, se ha realizado un estudio teórico de las propiedades del sulfuro de zinc, ZnS. Se ha observado cómo la celda primitiva de este material experimenta cambios con la presión, y dos fases que coexisten en el mismo intervalo de presiones. En el estudio hemos obtenido las gráficas de Energía-Volumen y Presión-Volumen para luego ajustarlas a ecuaciones de estado y así obtener algunas propiedades básicas. Además, hemos realizado un estudio del cambio que sufren las estructuras de ciertas fases observadas a distintas presiones junto con un análisis de la variación de la entalpía que nos permite obtener cuándo se produce este cambio de fases. Por último, realizamos un estudio de la estructura de bandas de las fases que se pueden encontrar en la ZnS.

In this work we have made a general study of the Density Functional Theory (DFT), in which we have centered our attention in the demonstrations of the theorems that lay the foundation of this theory. We have made a theoretical study of the properties of zinc sulfide using the program VASP that implements the DFT. In this material it can be observed how its primitive cell suffers a change when pressure is applied, in addition to this, two phases are observed that can be found in the same pressure range. In our study we have the graphics its Energy-Volume and Pressure-Volume curves which we have fitted with an equation of state to be able to obtain some basic properties. Furthermore, we have made a study of the changes that the structures of certain phases of the material undergoes with an analysis of the enthalpy variation that allows us to obtain when the changes in these phases take place. Lastly, we have made a study of the band structure of the phases that can be found for ZnS.

1   Objectives

The goal of this project is to introduce us to the Density Functional Theory, a theoretical approach to the study of materials that allows us to describe some important characteristics of the material, such us their bulk modulus and their band structure. We will also explain the basics of one of the programs that is used to apply the theory, the program VASP, so that can be later used to study the zinc sulfide, as an initiation to what a real study is made.

2   Introduction

Regarding solid-state physics and materials science, we have a different range of methods that allow us to study the properties of the atomics systems that conform the matter, in both theorical and computational approaches, to then compare the results with that obtained by experimentation. A method often used is the one that we are going to learn and applicate, known as the Density Functional Theory (DFT). To do this we will have to use a complex program known as *VASP*, that let us applicate the theory in a computational framework. In the next sections, we will try to explain the theory and the functioning of the program that had to be used later on for the study of the zinc sulfide, the material chosen for the initiation in this kind of studies.

3   Theoretical background

En esta sección realizamos un estudio detallado de la teoría en la que se fundamenta nuestro estudio, la DFT y los teoremas en los que se basa esta teoría. Además, introducimos los distintos archivos que se usan en el programa VASP, el cual es el que usaremos para realizar los cálculos de la siguiente sección, junto con la información que contienen cada uno y el uso que se le da. El texto bibliográfico utilizado en gran medida para realizar la sección sobre la teoría de la DFT ha sido la tesis doctoral del Dr. Andrés Mújica Fernaud, en la referencia [1], adicionalmente a las referencias [2, 4, 5].

3.1   Density Functional Theory (DFT)

Almost a century ago, Thomas and Fermi started what would be the first notions of the DFT during the 20's. They proposed an expression for the energy of an atom that has presents the kinetic energy as a function of the electronic density. Then, they combined this with the classical expression for the nucleon-electron and electron-electron interactions. [2] However, the precision of the values obtained was not as good as it should be. It was not until 1964 that there was formulated a theorical basis of the DFT with the Hohenberg-Kohn Theorem.

Before starting, I would like to give some context of the problem that we are going to resolve. The systems that we are going to deal with are composed by a great quantity of atoms and electrons with a dynamic that cannot be evaluated without considering both components.

Nevertheless, we can make an approximation in which the ions are constricted in a specific configuration (normally the equilibrium). This allows us to investigate their behavior separated and be able to consider only the dynamic of the electrons, best known as the Born-Oppenheimer approximation. By doing this, we now have an interacting many-bodies system that is, still, quite complex to resolve it directly. This is the reason why we need to use the DFT.

3.1.1 Hohenberg-Kohn Theorem

At the moment, this theorem was formulated for the first time when it was only valid for a rather simple system: spinless, non-degenerated, identical fermions interactuacting with an external field. Later in time it was extended to include a more complex variety of systems, although this is not important for the study that we are going to do. The Hohenberg-Kohn Theorem is constituted by two statements [3]:

I. ***Invertibility:*** The ground-state density of a many-particles system, $E[n(\mathbf{r})]$, can be used to get the external potential, $v_{ext}[\mathbf{r}]$, and with this, the system Hamiltonian, $\mid \Psi \rangle$, in a one-to-one correspondence:

$$n(r) \quad \leftrightarrows \quad v_{ext}[\mathbf{r}] \quad \leftrightarrows \quad \mid \Psi \rangle \tag{1}$$

II. ***Density Variational Principle:*** For a system of interactuacting fermions, there is an energy functional of the density, $n(\mathbf{r})$, whose minimum value can be deduced by the ground-state density and is the same in a many-electrons system.

$$E_v[n] = F[n] + \int n[\mathbf{r}]v_{ext}[\mathbf{r}]d^3\mathbf{r} \quad ; \quad F[n] = T[n] + V_{ee}[n] \tag{2}$$

where $T[n]$ is the kinetic energy operator and $V_{ee}[n]$ the electrons interactions operator.

We must demonstrate the validity of this theorem before we start to use it. To do this we are going to follow the proof by Levy [4], in which he defines a universal functional:

$$F[n] = \langle \hat{\Psi}[n] \mid T + V_{ee} \mid \hat{\Psi}[n] \rangle \tag{3}$$

The functional of the energy can be rewritten as:

$$\begin{aligned}
E_v[n] &= \langle \hat{\Psi}[n] \mid T + V_{ee} \mid \hat{\Psi}[n] \rangle + \langle \hat{\Psi}[n] \mid V_{ext} \mid \hat{\Psi}[n] \rangle = \\
&= \langle \hat{\Psi}[n] \mid H \mid \hat{\Psi}[n] \rangle = \\
&= \min_{\Psi \to n} \{ \langle \Psi \mid H \mid \Psi \rangle \}
\end{aligned} \tag{4}$$

According to the variational principle of Quantum Mechanics we can continue:

$$\begin{aligned}
\min_{n} \{ E_v[n] \} &= \min_{n} \left\{ \min_{\Psi \to n} \{ \langle \Psi \mid H \mid \Psi \rangle \} \right\} = \\
&= \min_{\Psi} \{ \langle \Psi \mid H \mid \Psi \rangle \} = E_0
\end{aligned} \tag{5}$$

For the density that minimizes the functional $E_v[n]$, n_0, we also have:

$$E_v[\hat{n}_0] = \langle \hat{\Psi}[\hat{n}_0] \mid H \mid \hat{\Psi}[\hat{n}_0] \rangle = \min_n \{E_v[n]\} = E_0 = \langle \Psi_0 \mid H \mid \Psi_0 \rangle \tag{6}$$

For this to be true, it is necessary that $\hat{\Psi}[n_0] \equiv \Psi_0$ and $\hat{n}_0 \equiv n_0$ to be true also, which ends the demonstration.

The functional that was defined by the Density Variational Principle, $F[n]$, is universal for every system because it does not depend on the external field. However, its form is unknown so we must make an approximation to use the theorem, in our case we will use the Kohn-Sham equations.

3.1.2 Kohn-Sham Equations

The core of this methos is the assumption that for every interacting system with a density $n(\mathbf{r})$, there must be a non-interacting system with the same density corresponding to a certain potential. This last system is called Kohn-Sham system [5]. The functional that we are going to use on this method can then be written as:

$$E_v[n] = F[n] + \int v[\mathbf{r}]n[\mathbf{r}]d^3\mathbf{r} \quad ; \quad F[n] = T_s[n] + E_H[n] + E_{xc}[n] \tag{7}$$

where $T_s[n]$ is the kinetic contribution to the ground-state energy of a reference fictitious system of non-interactuacting electrons with density n, E_H is the classical coulomb repulsion between two charge distributions of density n, and $E_{xc} = [E_{ee}[n] - E_H] + [T[n] - T_s]$ is the exchange-correlation energy. This equation is a reorganization of the function (2) defined in the Hohenberg-Kohn theorem, which is basically the same kind of problem to solve.

Applying the variational principal to the functional (7) we get the Euler-Lagrange for the density:

$$\frac{\delta T_s[n]}{\delta n(\mathbf{r})} + v_{eff}(\mathbf{r}) = \mu \quad \text{with the condition} \quad \int n(\mathbf{r})d\mathbf{r} = N \tag{8}$$

where the effective potential, v_{eff}, is the addition of the Hartree potential, $v_H(\mathbf{r})$, the potential that we had on the equation (7), and the exchange-correlation potential, $v_{xc}(\mathbf{r})$.

$$v_{eff} = v_H(\mathbf{r}) + v(\mathbf{r}) + v_{xc}(\mathbf{r}) = \int \frac{n(\mathbf{r'})}{|\mathbf{r} - \mathbf{r'}|}d\mathbf{r'} + v(\mathbf{r}) + \frac{\delta E_{xc}[n]}{\delta n(\mathbf{r})} \tag{9}$$

From the variational (8) we get the Kohn-Sham equations:

$$\left[-\frac{\hbar^2}{2m}\nabla^2 + v_{eff}[n](\mathbf{r}) \right] \psi_i(\mathbf{r}) = \epsilon_i \psi_i(\mathbf{r}) \quad ; \quad n(\mathbf{r}) = \sum_i |\psi_i(\mathbf{r})|^2 \tag{10}$$

where ϵ_i and $\psi_i(\mathbf{r})$ are the Kohn-Sham eigenvalues and eigenvector, respectively. The resolution of this system of Schrodinger equation's type, leads us to the form of $T_s[n]$:

$$T_s[n] = \sum_i \int \psi_i^*(\mathbf{r}) \left(-\frac{1}{2}\nabla^2 \right) \psi_i(\mathbf{r})d\mathbf{r} \tag{11}$$

The other terms regarding equation (7) can also be obtained in a satisfactory way in accordance with the density, except for the exchange-correlation energy for which we will need to

know an approximation for its value. To do this, we have a large quantity of methods but, in this work, we will use the *Local Density Approximation*, or LDA, that we will explain in the next section.

3.1.3 Local Density Approximation (LDA)

This is one of the many ways there are to approximate the exchange-correlation functional term that we had in equation (7):

$$E_{xc}^{LDA}[n] = \int \epsilon_{xc}^0(n(\mathbf{r}))n(\mathbf{r})d\mathbf{r} \quad ; \quad \epsilon_{xc}^0 = \epsilon_x^0 + \epsilon_c^0 \tag{12}$$

where ϵ_{xc}^0 the exchange-correlation energy density for an interacting homogeneous electron gas with density n. This can be seen as a sum of two parts: ϵ_x is the exchange density and ϵ_c is the one for the correlation. We know the analytical form for the first:

$$\epsilon_x = \frac{3e^2}{16\pi\epsilon_0 a_0 r_s} \left(\frac{9}{4\pi^2} \right)^{\frac{1}{3}} \tag{13}$$

For the correlation energy we do not have an analytical form that is valid for each density that can be interesting. To get this value we have some methods, though the most accurate is the one that uses the moments for a homogeneous gas of interactuacting electrons using the Monte Carlo Quantum method. A parameterization often used is the one made by Perdew and Zunger using the numeric study using the Monte Carlo method by Ceperley and Alder.

The Monte Carlo method can be reduced in a simple pattern: first, we define a domain of possible inputs, then we generate in it some random inputs from a probability distribution, next we must perform a deterministic computation on these inputs, and lastly, we aggregate the results. [6]

3.2 Crystalline Solid

Crystals are formed by a lattice created by three non-coplanar translational vectors called "lattice generators" $\mathbf{a_i}$, $i = 1, 2, 3$, and by a basis formed by the positions of the N_c atoms in the unit cell, τ_s, $s = 1, ..., N_c$. The ions that form the crystal can be found on the positions $\mathbf{R}_\alpha \equiv \mathbf{R_{m,s}} = \mathbf{R} + \tau_s$ where $\mathbf{R} = \sum_i m_i \mathbf{a_i}$, $m_i \in \mathbb{Z}$, are the lattice vectors. The form of the crystal is given by the repetition of the basis because the crystal has periodicity. However, when we get close to the surface this is lost. We can circumvent this by assuming that the material is infinity with periodic bounding conditions, so the wave functions must verify $\psi(\mathbf{r}+N_i\mathbf{a_i}) = \psi(\mathbf{r})$ with $N_1 N_2 N_3 = N$, $N_i \in N$, $N_i \sim N^{1/3}$ and $N \to \infty$, where N is the number of the cells in the crystal.

The Kohn-Sham equations on Dirac notation for crystals are:

$$\hat{h}_{KS}[n]|\psi_{n,\mathbf{k}}\rangle = \{\hat{t} + \hat{v}_{eff}[n]\}|\psi_{n,\mathbf{k}}\rangle = \epsilon_{n,\mathbf{k}}|\psi_{n,\mathbf{k}}\rangle \tag{14}$$

with $\hat{v}_{eff}[n] = \hat{v}_H[n] + \hat{v}_{xc}[n] + \hat{v}$ where $\hat{v} = \sum_{\mathbf{R}_\alpha} \hat{v}_\alpha[\mathbf{R}_\alpha]$ is the potential for the interaction between electron and the ions on the positions $\mathbf{R}_\alpha$. The form $\hat{v}_{scr}[n] = \hat{v}_H[n] + \hat{v}_{xc}[n]$ is the

screening potential and the effective potential, $\hat{v} + \hat{v}_{scr}$, is usually called screened potential. It is important to say that the potentials mentioned before have the same translational symmetry of the crystal. This implies that the eigenfunctions of the problem of Kohn-Sham eigenvalues problem are Bloch functions, $\psi_{n,\mathbf{k}}$, that verify:

$$\psi_{n,\mathbf{k}}(\mathbf{r} + \mathbf{R}) = e^{i\mathbf{k}\mathbf{R}}\psi_{n,\mathbf{k}}(\mathbf{r}) = e^{i\mathbf{k}(\mathbf{r}+\mathbf{R})}u_{n,\mathbf{k}}(\mathbf{r}) \quad ; \quad u_{n,\mathbf{k}}(\mathbf{r} + \mathbf{R}) = u_{n,\mathbf{k}}(\mathbf{r}) \tag{15}$$

where $\mathbf{k}$ is a vector in the first Brillouin zone. The eigenvalues $\epsilon_{n,\mathbf{k}} = \epsilon_n(\mathbf{k})$ form an energy band in the reciprocal space. The charge density is:

$$n(r) = \sum_{n,\mathbf{k}}^{oc.} |\psi_{n,\mathbf{k}}(\mathbf{r})|^2 = \sum_{\mathbf{k}}\sum_{n}^{oc.} |\psi_{n,\mathbf{k}}(\mathbf{r})|^2 = \frac{\Omega_c}{(2\pi)^3}\int_{\Omega_{Bz}} |p_{\mathbf{k}}(\mathbf{r})|^2 d\mathbf{k} \tag{16}$$

where $\Omega_c = \frac{\Omega}{N}$ is the volume of the unit cell. The sum of the quantum numbers n and k extends to every occupied monoelectronic level. To NN_e eigenstates of lower energy, where $N_e = \sum_s Z_s$ is the number of electrons by each cell and with Z_s the number of electrons of the ion that is on position s.

3.2.1 Kohn-Sham Equations and the total energy in the position representation

In this representation the equations take the form:

$$-\frac{\hbar^2}{2m}\nabla^2\psi_{n,\mathbf{k}}(\mathbf{r}) + \int v_{eff}[n](\mathbf{r},\mathbf{r'})\psi_{n,\mathbf{k}}(\mathbf{r'})d\mathbf{r'} = \epsilon_{n,\mathbf{k}}\psi_{n,\mathbf{k}}(\mathbf{r}) \tag{17}$$

with the density n given by the equation (16). The effective potential is:

$$v_{eff}[n](\mathbf{r},\mathbf{r'}) = \overbrace{[v_H[n](\mathbf{r}) + v_{xc}[n](\mathbf{r})]}^{v_{scr}(\mathbf{r})}\delta(\mathbf{r} - \mathbf{r'}) + v(\mathbf{r},\mathbf{r'}) = \tag{18}$$

$$= \left[v_H[n](\mathbf{r}) + v_{xc}[n](\mathbf{r}) + v^L(\mathbf{r})\right]\delta(\mathbf{r} - \mathbf{r'}) + \Delta v^{NL}(\mathbf{r},\mathbf{r'})$$

with:

$$v_H[n](\mathbf{r}) = \frac{e^2}{4\pi\epsilon_0}\int \frac{n(\mathbf{r'})}{|\mathbf{r} - \mathbf{r'}|}d\mathbf{r'} \tag{19}$$

$$v_{xc}[n](\mathbf{r}) = \frac{\delta E_{xc}[n]}{\delta n(\mathbf{r})} \simeq v_{xc}^{LDA}(n(\mathbf{r})) \tag{20}$$

and for the ionic potential being:

$$v(\mathbf{r},\mathbf{r'}) = \sum_\alpha v_\alpha[\mathbf{R}_\alpha](\mathbf{r},\mathbf{r'}) = \overbrace{\sum_\alpha v_\alpha^L[\mathbf{R}_\alpha](\mathbf{r})}^{v^L(\mathbf{r})}\delta(\mathbf{r} - \mathbf{r'}) + \overbrace{\sum_\alpha \Delta v_\alpha^{NL}[\mathbf{R}_\alpha](\mathbf{r},\mathbf{r'})}^{\Delta v^{NL}(\mathbf{r},\mathbf{r'})} \tag{21}$$

with:

$$v_\alpha(\mathbf{r},\mathbf{r'}) = v_\alpha^L(r)\delta(\mathbf{r} - \mathbf{r'}) + \underbrace{\sum_l \Delta v_{\alpha,l}^{NL}\delta(\mathbf{r} - \mathbf{r'})\sum_{m=-l}^{+l} Y_{lm}^*(\hat{r})Y_{lm}(\hat{r'})}_{\Delta v_\alpha^{NL}(\mathbf{r},\mathbf{r'})} \tag{22}$$

9

The expressions for $v_H[n](\mathbf{r})$, $v_{xc}[n](\mathbf{r})$ and $v(\mathbf{r}, \mathbf{r'})$ in a real space show in a clear way that the charge density, n, and the contributions of the effective potential are periodic. The potential of the coulomb interaction between ions has not been included in equation (18).

With this equation we can get the electronic energy using the expressions for the fundamental energy and adding the energy for the interaction between ions, E_{cc}

$$E = T_s + \overbrace{E_H + E_{xc}}^{E_{ee}} + \overbrace{E_{ec}^L + E_{ec}^{NL}}^{E_{ec}} + E_{cc} \tag{23}$$

where:

$$
\begin{aligned}
T_s &= \sum_{n,\mathbf{k}}^{oc.} \int \psi_{n,\mathbf{k}}^*(\mathbf{r}) \left(-\frac{\hbar^2}{2m} \nabla^2 \right) \psi_{n,\mathbf{k}}(\mathbf{r}) d\mathbf{r} \\
E_H &= \frac{1}{2} \int v_H[n](\mathbf{r}) n(\mathbf{r}) d\mathbf{r} = \frac{1}{2} \frac{e^2}{4\pi\epsilon_0} \int \int \frac{n(\mathbf{r})n(\mathbf{r'})}{|\mathbf{r} - \mathbf{r'}|} d\mathbf{r} d\mathbf{r'} \\
E_{xc} &= \int \epsilon_{xc}(n(\mathbf{r})) n(\mathbf{r}) d\mathbf{r} \\
E_{ec}^L &= \int v^L(\mathbf{r}) n(\mathbf{r}) d\mathbf{r} \\
E_{ec}^{NL} &= \sum_{n,\mathbf{k}} \int \int \psi_{n,\mathbf{k}}^*(\mathbf{r}) \Delta v^{NL}(\mathbf{r}, \mathbf{r'}) \psi_{n,\mathbf{k}}(\mathbf{r}) d\mathbf{r} d\mathbf{r'} \\
E_{cc} &= \frac{1}{2} \frac{e^2}{4\pi\epsilon_0} \sum_{\substack{\alpha,\beta \\ \alpha \neq \beta}} \frac{Z_\alpha Z_\beta}{|\mathbf{R}_\alpha - \mathbf{R}_\beta|}
\end{aligned}
\tag{24}
$$

E_H, E_{cc} y E_{ec}^L are individually divergent because of the large reach of the coulomb interaction. However, it is possible to demonstrate that these are mutually canceled (the first two are repulsive while the last is attractive) when we take in consideration the total sum. [1]

3.2.2 Kohn-Sham Equations and the total energy in the momentum representation

As we have mentioned before, the Kohn-Sham equations for a crystal corresponds to periodic potentials, this led to the conclusion that their eigenfunctions are Bloch wave functions. An adequate base for this problem is the one conformed by the plane waves, $|\mathbf{K}\rangle$; $\langle \mathbf{r}|\mathbf{K}\rangle = \frac{1}{\sqrt{\Omega}} e^{i\mathbf{K}\mathbf{r}}$, that already meet the periodic boundary conditions naturally. However, in most cases that can be interesting one needs an excessive number of plane waves to represent the oscillations on the charge density and potentials near the nucleus. So, we need to combine the PW method with the pseudo potentials method, which leads to numerous advantages: the convergence of the sums for the total energy is faster when we use pseudo potentials, we cannot add error when we move the origin because the plane waves are not selected to any specific origin point, and last, this formalism is easy enough to employ pre-existing codes, that allow us to resolve the problem efficiently.

Those terms that form the effective potential, $\hat{v}_{eff}$, have the translational symmetry of the lattice. In the basis that we have selected the only nonzero matrix elements of a single particle

operator $\hat{f}$ (non-local) which is periodic on positions, $f(\mathbf{r} + \mathbf{R}, \mathbf{r'} + \mathbf{R}) = f(\mathbf{r}, \mathbf{r'})$, belong to momentums $\mathbf{k} + \mathbf{G}$ and $\mathbf{k} + \mathbf{G'}$ that differ in a reciprocal lattice vector, $\mathbf{G} - \mathbf{G'}$:

$$\overbrace{f(\mathbf{k} + \mathbf{G}, \mathbf{k} + \mathbf{G'})}^{\langle \mathbf{k}+\mathbf{G}|\hat{f}|\mathbf{k}+\mathbf{G'}\rangle} = \frac{1}{\Omega} \int \int d\mathbf{r} d\mathbf{r'} \overbrace{f(\mathbf{r}, \mathbf{r'})}^{\langle \mathbf{r}|\hat{f}|\mathbf{r'}\rangle} e^{-i(\mathbf{k}+\mathbf{G})\mathbf{r}} e^{i(\mathbf{k}+\mathbf{G'})\mathbf{r'}}$$

$$f(\mathbf{r}, \mathbf{r'}) = \int_{\omega_{B_z}} d\mathbf{k} \sum_{\mathbf{G}, \mathbf{G'}} f(\mathbf{k} + \mathbf{G}, \mathbf{k} + \mathbf{G'}) e^{i(\mathbf{k}+\mathbf{G})\mathbf{r}} e^{-i(\mathbf{k}+\mathbf{G'})\mathbf{r'}} \tag{25}$$

For a local operator, $f(\mathbf{r}, \mathbf{r'}) = f(\mathbf{r})\delta(\mathbf{r} - \mathbf{r'})$, and then $f(\mathbf{k} + \mathbf{G}, \mathbf{k} + \mathbf{G'}) \equiv f(\mathbf{G} - \mathbf{G'})$, independently of $\mathbf{k}$, where $f(\mathbf{G})$ denote the components of the Fourier expansion of $f(\mathbf{r})$.

Projecting the equations (14) over the plane waves basis and using the relation that we wrote before; we get the next expressions for the reciprocal space:

$$\sum_{\mathbf{G'}} \underbrace{\left[\left(-\frac{\hbar^2}{2m} |\mathbf{k} + \mathbf{G}|^2 \delta(\mathbf{G}, \mathbf{G'}) + v_{eff}(\mathbf{k} + \mathbf{G}, \mathbf{k} + \mathbf{G'}) \right) \right]}_{H_{\mathbf{G},\mathbf{G'}}(\mathbf{k}) - \epsilon_n(\mathbf{k})\delta(\mathbf{G},\mathbf{G'})} c_{n,\mathbf{k}}(\mathbf{G'}) = 0 \tag{26}$$

with:

$$v_{eff}(\mathbf{k} + \mathbf{G}, \mathbf{k} + \mathbf{G'}) = v_H(\mathbf{G} - \mathbf{G'}) + v_{xc}(\mathbf{G} - \mathbf{G'}) +$$
$$+ \underbrace{v^L(\mathbf{G} - \mathbf{G'}) + \Delta v^{NL}(\mathbf{k} + \mathbf{G}, \mathbf{k} + \mathbf{G'})}_{v(\mathbf{k}+\mathbf{G},\mathbf{k}+\mathbf{G'})} \tag{27}$$

where $c_{n,\mathbf{k}}(\mathbf{G}) \equiv c_n(\mathbf{k} + \mathbf{G})$ are the coefficients of the expression of the Bloch wave $\psi_{n,\mathbf{k}}$ eigenfunction in the plane wave basis:

$$\psi_{n,\mathbf{k}}(\mathbf{r}) = e^{i\mathbf{k}\mathbf{r}} u_{n,\mathbf{k}}(\mathbf{r}) = \sum_{\mathbf{G}} c_{n,\mathbf{k}}(\mathbf{G}) e^{i(\mathbf{k}+\mathbf{G})\mathbf{r}} \tag{28}$$

The screening potential that we defined before, v_{scr}, depends on the electronic density, n, and the Kohn-Sham equations, equation (26), must be solved self-consistent. The density function, n, is periodic and, in terms of the occupied levels of the wave function $c_{n,\mathbf{k}}(\mathbf{G})$, the coefficient of the Fourier development has the form:

$$n(\mathbf{G}) = \sum_{n,\mathbf{k}}^{oc.} \sum_{\mathbf{G'}} c_{n,\mathbf{k}}^*(\mathbf{G'}) c_{n,\mathbf{k}}(\mathbf{G} + \mathbf{G'}) \tag{29}$$

If we do Fourier transformation on the equation (19) for the Hartree potential, we get the relation between the components n and v_H in the reciprocal space:

$$v_H(\mathbf{G}) = \frac{e^2}{\epsilon_0} \frac{n(G)}{|\mathbf{G}|^2} \tag{30}$$

For the exchange-correlation potential, it is useful to evaluate $v_{xc}(\mathbf{G})$ firstly doing the calculation of $n(\mathbf{r})$ in a unit cell lattice. Next, we calculate $v_{xc}(\mathbf{r})$ using equation (20) and, lastly, we must do the Fourier transformation of $v_{xc}(\mathbf{r})$. If we follow the same steps, we can get $\epsilon_{xc}(\mathbf{G})$.

The ionic potential $v(\mathbf{k} + \mathbf{G}, \mathbf{k} + \mathbf{G'})$ has no dependence with the charge distribution n, this means that it has to be evaluated only at the beginning of our calculations. According to the

equation $v^L(\mathbf{r}) = \sum_{\mathbf{R},s} v_s^L(|\mathbf{r} - (\mathbf{R} + \tau_s)|)$ we get:

$$v^L(\mathbf{G}) = \frac{1}{\Omega} \int_\Omega d\mathbf{r} v^L(\mathbf{r}) e^{-i\mathbf{G}\mathbf{r}} = \sum_s e^{-i\mathbf{G}\tau_s} v_s^L(\mathbf{G}),$$

$$v_s^L(\mathbf{G}) = v_s^L(|\mathbf{G}|) = \frac{1}{\Omega} \int_\Omega d\mathbf{r} v_s^L(\mathbf{r}) e^{-i\mathbf{G}\mathbf{r}} \tag{31}$$

where $v_s^L(\mathbf{R})$ is the Fourier transformation of the local component for the ionic potential associated with the position τ_s, that depends only on the atom type that it is occupying. For the non-local component $\Delta v^{NL}(\mathbf{r},\mathbf{r'}) = \sum_{\mathbf{R},s} \sum_l \Delta v_{s,l}^{NL}[\mathbf{R} + \tau_s](\mathbf{r},\mathbf{r'})$ we have:

$$\Delta v^{NL}(\mathbf{k}+\mathbf{G},\mathbf{k}+\mathbf{G'}) = \frac{1}{\Omega} \int \int d\mathbf{r} d\mathbf{r'} \Delta v^{NL}(\mathbf{r},\mathbf{r'}) e^{-i(\mathbf{k}+\mathbf{G})\mathbf{r}} e^{i(\mathbf{k}+\mathbf{G'})\mathbf{r'}}$$

$$= \sum_s e^{i(\mathbf{G}+\mathbf{G'})\tau_s} \sum_l \Delta v_{s,l}^{NL}(\mathbf{k}+\mathbf{G},\mathbf{k}+\mathbf{G'}) \tag{32}$$

$$\Delta v_{s,l}^{NL}(\mathbf{k}+\mathbf{G},\mathbf{k}+\mathbf{G'}) = \frac{1}{\Omega} \int \int d\mathbf{r} d\mathbf{r'} \Delta v_{s,l}^{NL}(\mathbf{r},\mathbf{r'}) e^{-i(\mathbf{k}+\mathbf{G})\mathbf{r}} e^{i(\mathbf{k}+\mathbf{G'})\mathbf{r'}}$$

where the component I of the non-local part of the types of ion potential have the semi-local forma $\Delta v_{s,l}^{NL}(\mathbf{r},\mathbf{r'}) = \Delta v^{NL}(r)\delta(r - r')P_l(\hat{\mathbf{r}},\hat{\mathbf{r'}})$.

In momentum representation, the contributions to the total electronic energy that appear in equation (24) have the expressions:

$$T_s = \Omega \frac{\hbar^2}{2m} \sum_{n,\mathbf{k}} \sum_{\mathbf{G}} |\mathbf{k}+\mathbf{G}|^2 |c_{n,\mathbf{k(G)}}|^2$$

$$E_H = \Omega \frac{1}{2} \sum_{\mathbf{G}} n^*(\mathbf{G}) v_H(\mathbf{G}) = \Omega \frac{1}{2} \frac{e^2}{\epsilon_0} \sum_{\mathbf{G}} \frac{|n(\mathbf{G})|^2}{|\mathbf{G}|^2}$$

$$E_{xc} = \Omega \sum_{\mathbf{G}} n^*(\mathbf{G}) e_{xc}(\mathbf{G})$$

$$E_{ec}^L = \Omega \sum_{\mathbf{G}} n^*(\mathbf{G}) v^L(\mathbf{G}) \tag{33}$$

$$E_{ec}^{NL} = \Omega \sum_{n,\mathbf{k}} \sum_{\mathbf{G},\mathbf{G'}} c_{n,\mathbf{k}}^*(\mathbf{G}) c_{n,\mathbf{k}}(\mathbf{G'}) \Delta v^{NL}(\mathbf{k}+\mathbf{G},\mathbf{k}+\mathbf{G'})$$

$$\Delta E_{xc} = \Omega \sum_{\mathbf{G}} n^*(\mathbf{G}) (\epsilon_{xc}(\mathbf{G}) - v_{xc}(\mathbf{G}))$$

$$E_{cc} = \frac{1}{2} \frac{e^2}{4\pi\epsilon_0} \sum_{\substack{\alpha,\beta \\ \alpha \neq \beta}} \frac{Z_\alpha Z_\beta}{|\mathbf{R}_\alpha - \mathbf{R}_\beta|} = N \frac{1}{2} \frac{e^2}{4\pi\epsilon_0} \sum_{\mathbf{R},s,s'} \frac{Z_s, Z_{s'}}{|\mathbf{R} + (\tau_s - \tau_{s'})|}$$

The sum on the last member of E_{cc} excludes the case $s = s'$ when $\mathbf{R} = 1$. The charge density is a real quantity, $n^*(\mathbf{R}) = n(-\mathbf{R})$.

Integrals in reciprocal space

As we have seen, when we use the Kohn-Sham equations to crystals it appears the necessity to integrate periodic functions on $\mathbf{k}$-space, $g(\mathbf{k} = g(\mathbf{k}) + \mathbf{G})$, like the band energy, $\epsilon_n(\mathbf{k}) \equiv \epsilon_{n,\mathbf{k}}$, or the particle density, $n_k(\mathbf{r})$. The integral can be reduced to the first Brillouin zone thanks to the periodicity of the function $g(\mathbf{k})$, which can later be approximated to a discreet sum on a

set of special points, $\mathbf{k}_i$, and weights, w_i, $\{\mathbf{k}_i, w_i\}$:

$$\frac{1}{\Omega_{B_z}} \int_{\Omega_{B_z}} d\mathbf{k} g(\mathbf{k}) \approx \sum_i w_i g(\mathbf{k}_i) \tag{34}$$

where $\sum_i w_i = 1$. Equation (34) corresponds to the $\mathbf{R} = 0$ of the Fourier expansion of the periodic function, $g(\mathbf{k}) = \sum_{\mathbf{R}} g(\mathbf{R}) e^{ik\mathbf{R}}$, with $\mathbf{R}$ vectors of the direct lattice. Therefore, if the set of special points exactly integrates the terms $e^{i\mathbf{k}\mathbf{R}}$, $\sum_i w_i e^{ik_i\mathbf{R}} = 0$ for every $\mathbf{R}$ except $\mathbf{R}_0 = 0$, the expression (34) gives the exact value for the integration of $g(\mathbf{k})$.

Cutoff of the plane waves base

In every algorithm that use the expansion of a function we need to establish a *cutoff* to end it. On the problem we have, this is put in relation to the kinetic energy of the plane waves that are used on the momentum representation. This leads to a development of the functions, $\psi_{n,\mathbf{k}}$, that only have plane waves $|\mathbf{k} + \mathbf{G}\rangle$ with kinetic energy E_c, $\frac{\hbar^2}{2m}|\mathbf{k} + \mathbf{G}|^2 \leq E_c$. These are the vectors $\mathbf{G}$ of the reciprocal lattice inside a sphere of ratio $G_c = \left(\frac{2m}{\hbar^2} E_c\right)^{1/2}$ centered at $\mathbf{k}$. The number of vectors $\mathbf{G}$ that comply with this condition, $N_{pw}(\mathbf{k})$, depends on the vector $\mathbf{k}$ for which one is solving the Kohn-Sham equations. However, $\mathbf{k}$ is a vector within the first Brillouin zone and in practice $|\mathbf{k}| \ll G_c$ and the dependence on $\hat{(}h$ is not really important. N_{pw} can be estimated multiplying the volume of the cut off sphere of ratio G_c by the vector density on the reciprocal lattice, $\Omega_c/(2\pi)^3$: $N_{pw} \approx \frac{1}{6\pi^2}\left(\frac{2m}{\hbar^2}\right)^{3/2} E_c^{3/2}\Omega_c$. N_{pw} is the dimension of the matrix $\mathbf{H}_{\mathbf{G},\mathbf{G}'}(\mathbf{k})$ whose diagonalization gives the energies $\epsilon_{n,\mathbf{k}}$ and the momentum representation of the functions $\psi_{n,\mathbf{k}}$.

3.3 VASP

In order to applicate the theory explained before we are going to use the Viena Ab Initio Simulation Package [7], or $VASP$ [8], that allow us to implement the DFT methodology in a scheme of pseudopotentials and a basis of plane waves. To start the simulations, we need four different input files:

- **POSCAR:** This file contains the information of the structural data of the material we are investigating. It also has de basis vectors and the positions of the atoms, both of them can and need to be modified according to the phase want to explore.

- **POTCAR:** This one contains the pseudopotential for each atomic species used in the simulation. If this number is higher than one, then the POTCAR files can be concatenated in the same order found in the other files. This is the only file that will not be modified in our study.

- **KPOINTS:** This file has the grid for the Brillouin zone integration. In this study we used two main options to describe the Bloch vector (k-vectors): the first one is to introduce the spacing of the mesh and choose a method to create them (we used this in the majority of the project) or introduce it manually (this one was used exclusively for the calculations of the bandgaps).

- **INCAR:** This file is the one with all the instructions for the simulation, such us the cutoff energy in the plane wave expansion or the method used to integrate the mesh in the KPOINTS file.

As we might notice, all of the files (except the POTCAR) will be modified during our study in a way or the other. What changes had to be done and why will be explained in each section. Once we run the program, we obtain different output files and the most important in this work were:

- **CONTCAR:** This file contains a relaxed cell in POSCAR format that can be used as the POSCAR for the next step in the calculation, pertaining to the optimized structure.

- **OUTCAR:** This file gives detailed output of a VASP run, including dielectric properties, forces on the atoms, etc. It is from this file that we take the energy and the pressure for the cell after running VAPS.

- **CHGCAR:** This file containd the charge density necessary to make the calculations of the band structures.

- **DOSCAR:** In this file we have the Fermi energy and the density of states that can be found represented in the section of the band structures.

4 Results for the study of Zinc Sulfide

A continuación se realiza el estudio del material escogido, el sulfuro de zinc. En este apartado comenzamos con una introducción a las características del material, para continuar con el estudio teórico haciendo uso del VASP. Comenzamos el estudio con la obtención de la ecuación de estado a través de la representación de Energía-Volumen, de la que obtenemos el módulo de comprensibilidad y el volumen de equilibrio. Una vez hecho esto estudiamos cómo varían las estructuras de las fases no cubicas con respecto al volumen de la celda, y a qué presión se producen los dos cambios de fases experimentalmente observados en este material. Terminamos estudiando las estructuras de bandas de las distintas fases.

Zinc sulfide is vastly used in technology where it is known for its phosphorescence. [9] This is going to be the material we are going to analyze at normal and high-pressure conditions for its many interesting properties at a crystallographic point of view. At normal conditions ZnS can be found in two structures: Zincblende, which has a cubic cell with space group $F\bar{4}3m$, and Wurtzite, which has a hexagonal cell with space group $P6_3mc$. Both of them can be found in Nature. If we increase the pressure applied to our compound, we can get to the Rocksalt structure, a cubic cell with space group $Fm\bar{3}m$, and if we keep augmenting the pressure, we will then get the Cmcm phase, which is orthorhombic [10]. All of this is summarized in Figure 1.
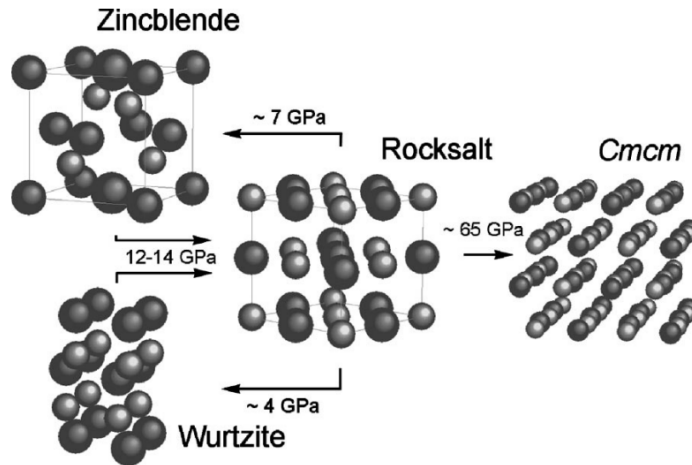

Figure 1: Different structures adopted by ZnS under different pressure conditions.

Before we can start studying the properties of the phases, such as the equilibrium volume or the pressure range of stability, we must first study the convergence of the energy with the cutoff energy and the number of integration points chosen on the Brillouin zone (which we will call the integration grid from now on) to put them in the best values for the rest of the calculations. This should be done with every phase that we want to study, but we only did this part for Zincblende for which the variation in the cutoff and the grid were taken as reference for the other phases (the grid for the Cmcm phase was 20x20x20, and for the Wurtzite phase we used 18x18x12).

We started calculating the convergence with respect to the cutoff energy. For this we start fixing the value of the grid (in our case we used 8x8x8) and volume (we did not modify the POSCAR file for the study of the convergence). The next step is to use different cutoffs (from 200 eV to 400 eV) and represent the variation in pressure and energy for each of them. The result can be observed in Figure 2.
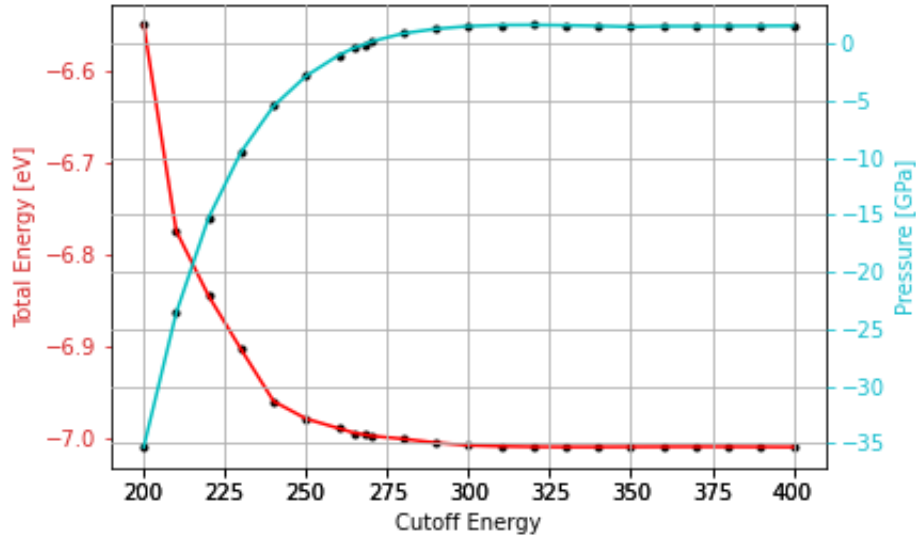

Figure 2: Variation of the total energy and the pressure of Zincblende with the cutoff energy.

For the calculation of the convergence with respect to the grid we used the same idea that before: we fixed the cutoff energy (in this case we used 364 eV) and, without modification of the POSCAR file, we changed the size of the integration grid. In this case the values used can be seen in Figure 3.
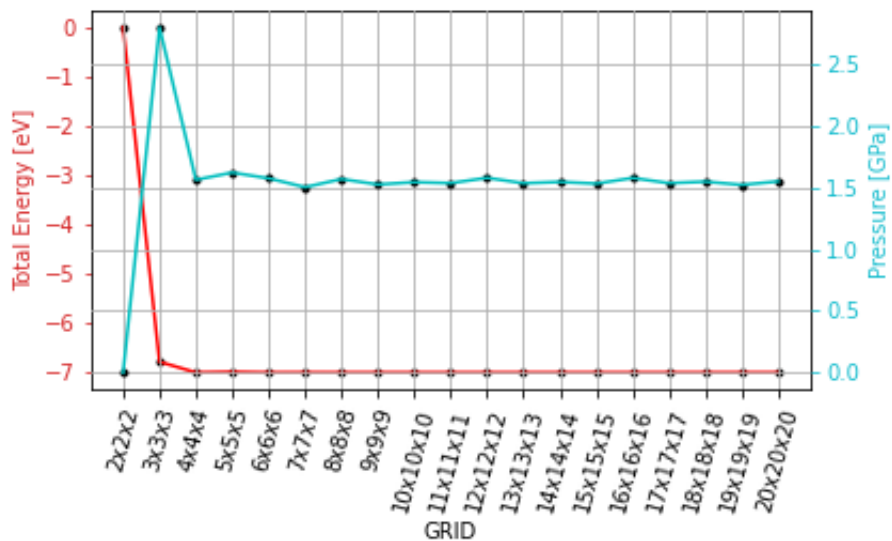
Figure 3: Variation of the total energy and the pressure of Zincblende with the size of the integration grid.

In both Figures we can observe how both values get into a plateau. From this range we have to choose the value for the cutoff and the grid for the rest of the calculations, and in our case we decided to use a cutoff energy of 364 eV and a grid of 8x8x8 for Zincblende and one of 20x20x20 for Rocksalt phase because of its metallic behaviour (the grid for Cmcm and Wurtzite were mentioned before).

4.1 Birch-Murnaghan equation of state

With this data we can proceed with the necessary simulations to obtain the equation of state for every phase. First of all, we have to study the variation in the energy and pressure with the volume, for this we must create different POSCAR files with the only variation between them being the volume and run VASP. The time that it takes to obtain the results depends on a lot in the cell under study. For example, the Cmcm phase took more than 24 hours with one processor for each POSCAR file (later on we used more than one) but Zincblende took less than 10 min for all of them. This is something that should be taken into consideration when making this kind of process.
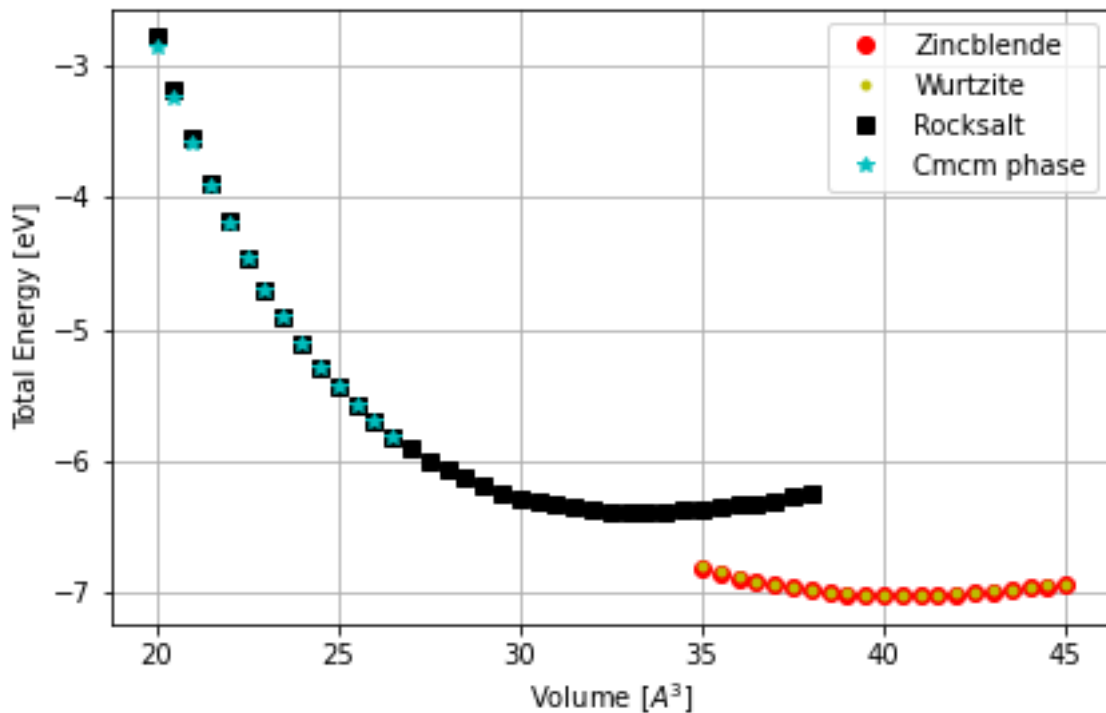

Figure 4: Calculated Energy-Volume curves for the phases under consideration.

From Figure 4 we can obtain some really important information that agrees with the basic information that we know when we started this study. First of all, the curves for Zincblende and Wurtzite are both almost indistinguishable from one another which agrees with the experimental observation that both phases coexist in the same range of low pressures. In the energies for the other phases can be observed an appreciable difference.
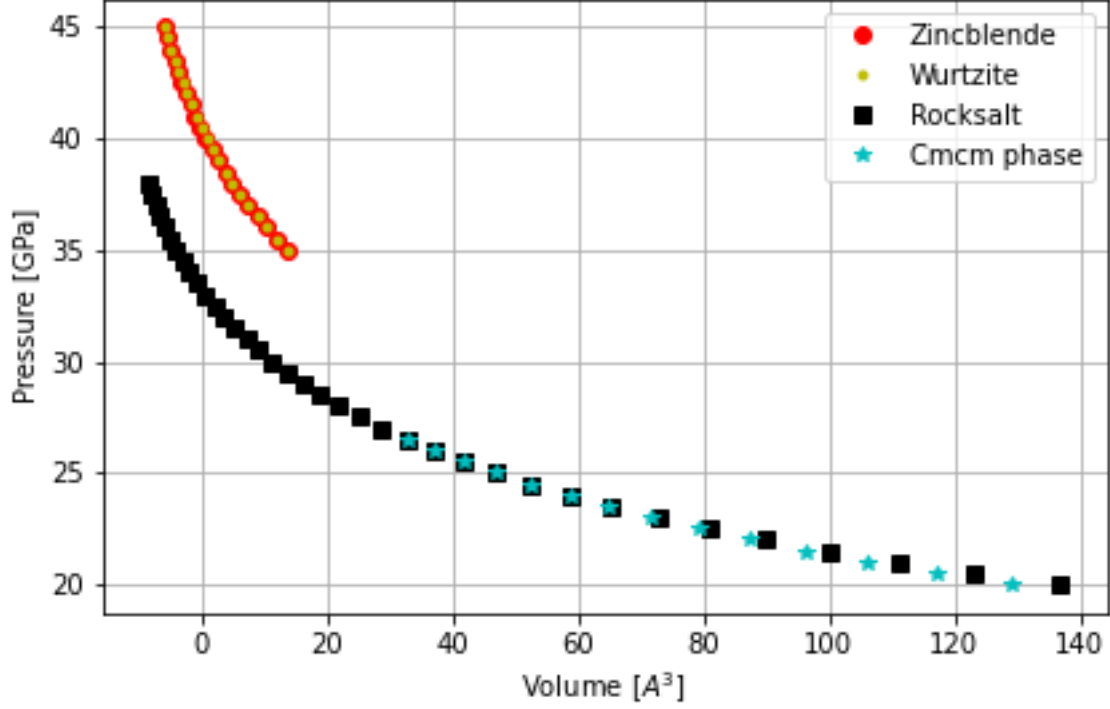
Figure 5: Calculated Pressure-Volume curves for the phases under consideration.

In Figure 5 the differentiation at high pressures that happen between the Rocksalt and Cmcm phase is clearer. This figures also give us the idea that for smaller pressures the Cmcm phase turn into a Rocksalt phase or similar which is an interesting detail that will be discussed later.

To extract the different properties from these graphics we need to obtain their equation of state, which is an equation that let describes the state of matter under a given set of physical conditions. In this case we will use the Birch-Murnaghan equation of state, published in 1947, that makes a relation between internal energy and volume, and between the pressure and volume (we consider $T = 0$): [11]

$$P(V) = \frac{3B_0}{2} \left[\left(\frac{V}{V_0} \right)^{\frac{7}{3}} - \left(\frac{V}{V_0} \right)^{\frac{5}{3}} \right] \left\{ 1 + \frac{3}{4} \left(B_0' - 4 \right) \left[\left(\frac{V}{V_0} \right)^{\frac{2}{3}} - 1 \right] \right\} \tag{35}$$

$$E(V) = E_0 + \frac{9V_0 B_0}{16} \left\{ \left[\left(\frac{V}{V_0} \right)^{\frac{2}{3}} - 1 \right]^3 B_0' + \left[\left(\frac{V}{V_0} \right)^{\frac{2}{3}} - 1 \right]^2 \left[6 - 4 \left(\frac{V}{V_0} \right)^{\frac{2}{3}} \right] \right\} \tag{36}$$

where E_0 is the energy at equilibrium (zero pressure), V_0' is the equilibrium volume, B_0 is the bulk modulus at equilibrium and B_0' is the first derivate of B_0 with respect to pressure. The Equation (36) is found by integration of the Equation (35). To fit the data with Equation (36) we created a program in python that gave us the next graphics:
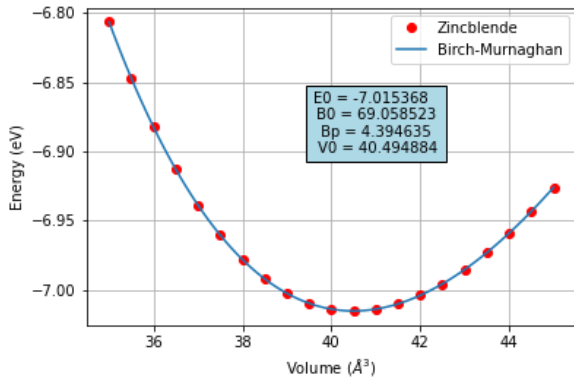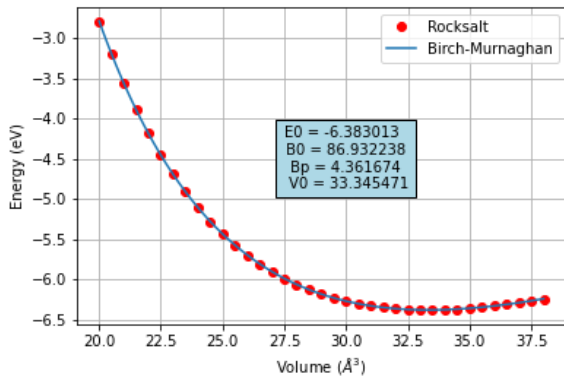
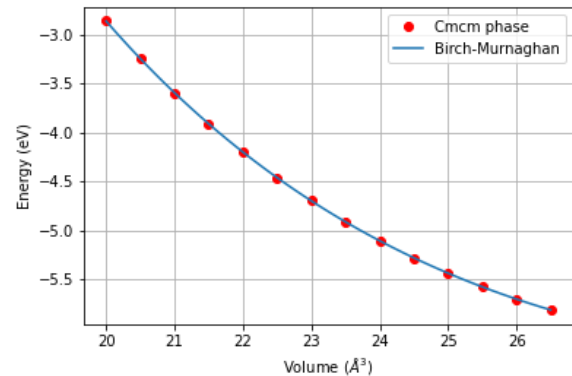(a) Energy variation with the volume for the Zincblende Structure.
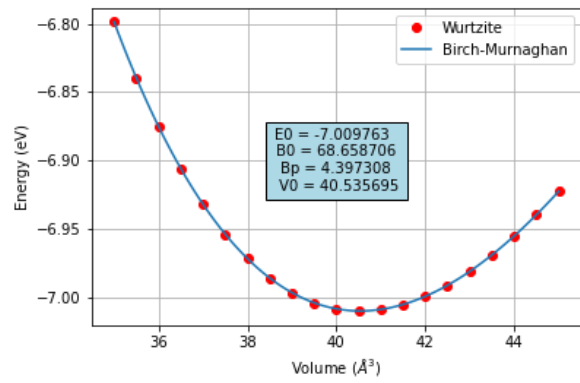
(b) Energy variation with the volume for the Wurtzite Structure.

Figure 6: Results of the fitting of the energy-volume curves with the Birch-Murnaghan equation of states for the low pressure.

In Figure 6 can be seen the fittings for Zincblende and Wurtzite. As expected, the values to the four parameters are similar with little differences.

(a) Energy variation with the volume for the Rocksalt Structure.

(b) Energy variation with the volume for the Cmcm phase Structure.

Figure 7: Results of the fitting of the energy-volume curves with the Birch-Murnaghan equation of states for the high pressure.

In Figure 7 we have represented the data given by the program for the Rocksalt and the Cmcm phase. The data for the Cmcm phase is not present because its behaviour at a lower pressure is the same as the Rosksalt phase and, as we mentioned before, the Birch-Murnaghan equation represents the states at $0 GPa$.

We compare now the data obtained in this work with the ones expected by previous theoretical and experimental work. The value E_0 cannot be checked because it is not a data that is usually obtained so we do not have a database to compare it, but it can also be found in the next table:

		$E_0[meV]$	$V_0[\dot{A}^3]$	$B_0[GPa]$	B_0'
Theoretical		$-$	37.7^b	84.2^b	4.3^b
Experimental	Zincblende	$-$	38.9^a	79.5^a	4^a
This Work		0	40.49	69.05	4.39
Theoretical		$-$	$-$	$-$	$-$
Experimental	Wurtzite	$-$	39.2^a	80.1^a	4^a
This Work		6	40.53	68.65	4.39
Theoretical		$-$	31.0^b	105.3^b	4.3^b
Experimental	Rocksalt	$-$	31.6^a	96.7^a	4.3^a
This Work		633	33.34	86.93	4.36

Table 1: Parameters of the fitting of the energy-volume curves of the studies phases to a Birch-Murnaghan equation of state. The values of E_0 are given with respect to the zincblende phase. *a) Ref. [10] b) Ref. [12]*

Theoretical data for the Wurtzite was not found for this material. Nevertheless, our data is relatively close to the ones that were expected for every phase. The parameters that have a largher difference are the B_0 and the B_0' but they are in an acceptable range. As it can be observed, the energy at equilibrium, E_0, increase when go from the phases at lower pressures to the phases at higher ones.

4.2 Structural Parameters

In the next section we will make a study about how the internal structure can change with the volume. For this we will represent the values of the structural parameters obtained from the relaxed structure found in the CONTCAR file. Once we have the relaxed structure, we can use FYNDSIM [13], an internet program that allows us to find the symmetry of a crystal. This study will only be done for two of the four phases that can be found in ZnS, the Cmcm and Wurtzite phases. We will not make a study for Rocksalt and Zincblende because there is not a change of their structural parameters with pressure for either of them.

First of all, we will make an introduction to the forms of the structures that we are going to talk about and what we call internal and structural parameters. In Figures 8a and 8b we can observe the primitive cell of the phases under study represented using the program VESTA. From now on, we will call structural parameters to the values of a, b and c that defines our cell.
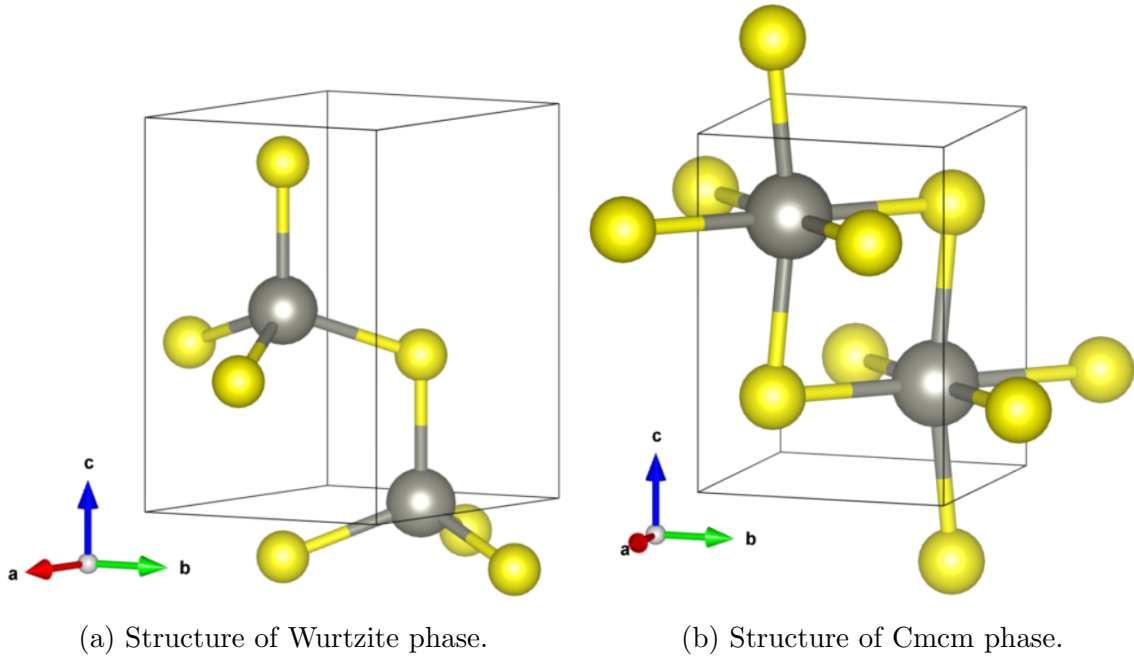
(a) Structure of Wurtzite phase.　　　　(b) Structure of Cmcm phase.

Figure 8: Representation of the structures used in this section. The arrow a goes in the direction of x, b in the direction of y and cc in the direction of z.

As we know, the structures in crystallography are classified in space groups that represent a description of the symmetry of the crystal. The notation used in this project is the Hermann-Mauguin notation, also called international notation, which has the advantage of being used in different data base, such us in Reference [14]. For Wurtzite phase we can obtain the coordinates for the atoms present in the reference cited before, these are $(\frac{1}{3}, \frac{2}{3}, z)(\frac{2}{3}, \frac{1}{3}, z + \frac{1}{2})$, where we have z as the special parameter that we will represent later. For Cmcm phase we have $(x, y, \frac{1}{4})(-x, -y, \frac{3}{4})(-x, y, \frac{1}{4})(x, -y, \frac{3}{4})$, with x and y being the special parameters in this phase.

We will now start with the representations of the different parameters presented until now and their change with compression.
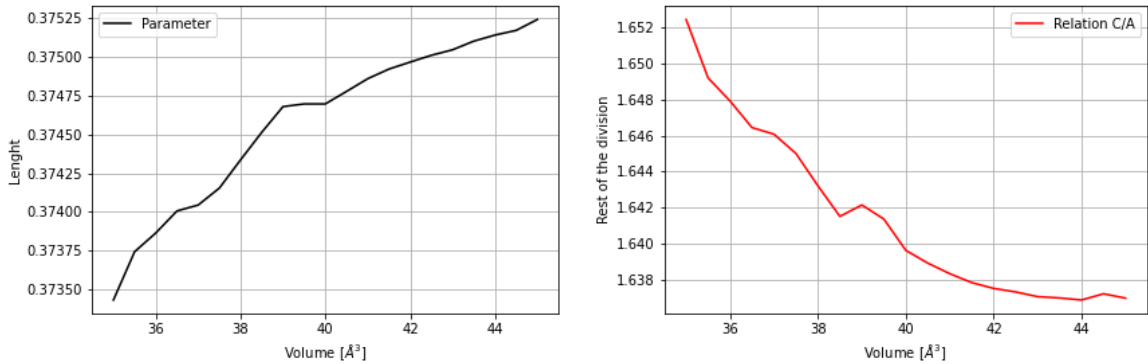
(a) Representation of the change in the special parameters with the compression.　(b) Representation of the change in the structure parameters with the compression.

Figure 9: Evolution with pressure of the structural parameters of the Wurtzite phase.

In Figure 9a we can observe how the special parameter for the Wurtzite phase does not get to a plateau at large volumes (low and negative pressures) point in contraposition for the c/a ratio represented in Figure 9b.
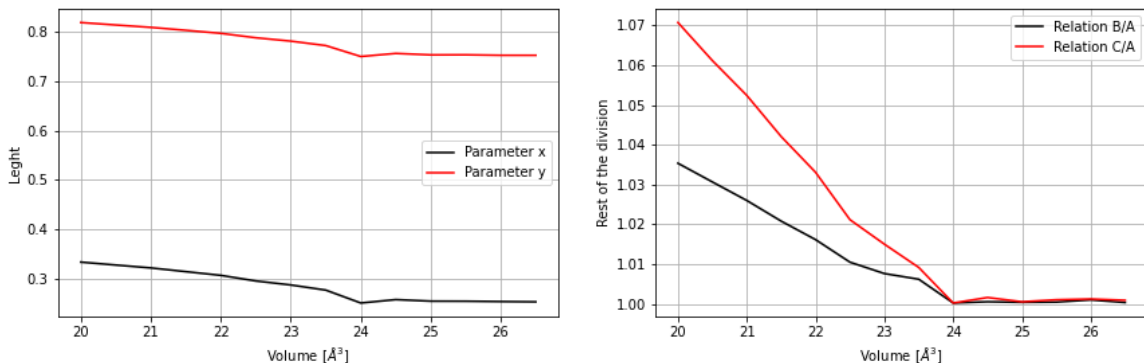
(a) Representation of the change in the special parameters with the compression.

(b) Representation of the change in the structure parameters with the compression.

Figure 10: Evolution with pressure of the structural parameters of the Cmcm phase.

In Figure 10 we have represented the variation of the parameters of the Cmcm phase. As it can be seen, the cell parameters transform at lower pressures from an orthorhombic cell into a cubic cell, this was expected as it could be observed in Figure 4 and 5 that the Cmcm phase turned into the Rocksalt phase in this scenario. Starting in Cmcm at high pressure, the rocksalt structure appears when the pressure is reduced and corresponds to $x \approx 0.75$ and $y \approx 0.25$. All of these results are consistent with the behavior observed and the information consulted. [15]

4.3 Phase transformation.

At Figure 1 we gave a representation of the different phase transformations that can occur in zinc sulfide. In this section we will study for which pressure applied to the crystal the transformation occur. To do this we have to study the change in enthalpy per atom with pressure. The enthalpy (zero temperature is assumed) is given by:

$$H = E + V \cdot P \tag{37}$$

Where H is the enthalpy, V is the volume per atom, P is the pressure obtained as $-\frac{dE}{dV}$ and E is the energy per atom.

First of all, we must calculate the enthalpy using Equation (37) for every phase except Wurtzite, this one will not be done because it has almost the same behavior as Zincblende. After this we interpolate the results and calculate $\Delta = H_2 - H_1$, where H_1 and H_2 are the two phases from which we want to obtain the transition. In this case we only need to consider two transformations, from Zincblende to Rocksalt, and from Rocksalt to Cmcm, so what we are representing is the change in enthalpy from the first phase to the other one, when we observe that they cross paths then it is at that point where we can locate the transition.
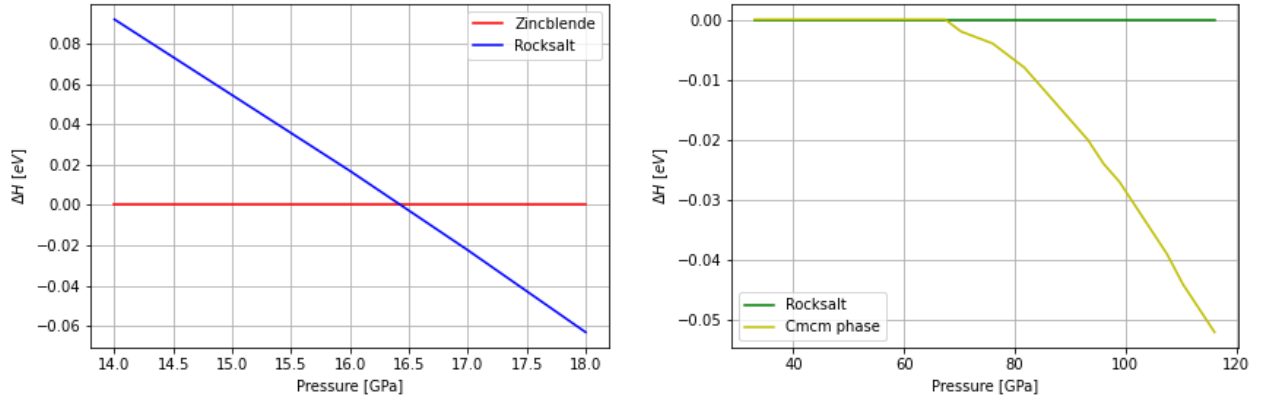
(a) Difference between the enthalpies of Zincblende and Rocksalt phases.

(b) Difference between the enthalpies of Rocksalt and Cmcm phases.

Figure 11: Comparison between enthalpies found in different phases.

In Figure 11 we can observe what we mentioned before, both of them give us the point where the transformation is made. There are some peculiarities on both graphics that I would like to highlight; the first one is that on Figure 11a we have clear a cross between them but that is all, this is what we expected because zincblende does not transform continously into Rocksalt as pressure is increased (the transition is strongly first order). The second one is the almost continously evolution of a Cmcm phase from the Rocksalt phase observed in Figure 11b, and in line with the data in Figures 4 and 5. Here, previous theoretical and experimental studies report a second order of weakly first order transition, associated to a local instability of the Rocksalt phase as pressure increases. [16]

Phase transition	This work [GPa]	Bibliography [GPa]
ZB to RS	16.45	15.9[a]
RS to Cmcm	67.40	~ 65[b]

Table 2: Calculated transition pressures. *a) Ref. [17] b) Ref. [15]*

All of the data can be taken from this graphics is summarized in Table 2, where we can also find the expected values for them. Our data are quite similar to the one that we found in the bibliography, both of them are less than 3 GPa from the expected value.

4.4 Band Structure

In this section we will study the electronic band structure of the different phases. The band structure describes the range of energy levels that electrons may have within it, as well as possible a range of prohibited energies, called the bandgap. To obtain the band structure of our phases we had to introduce the special K-points path [18] and change some commands in the INCAR file that will tell the program VASP to calculate the bands, after this we can start running the program.
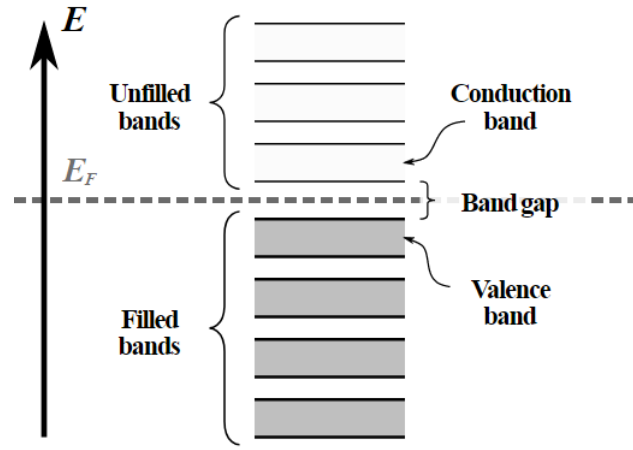
Figure 12: Representation of a semiconducting band structure.

In Figure 12 we can observe a representation of what we will be looking at in this section. There are two important concepts in this image that we will be using in the next pages, the Fermi energy, E_F, represented as a dashed line, which is the energy of the highest occupied level by an electron in our material. The other concept is the *Band gap*, which is the separation that can be found between the conduction and the valence band in semiconducting materials. If the Fermi energy is located in a band gap the material is insulating (or semiconducting) while it is metallic otherwise. [19]
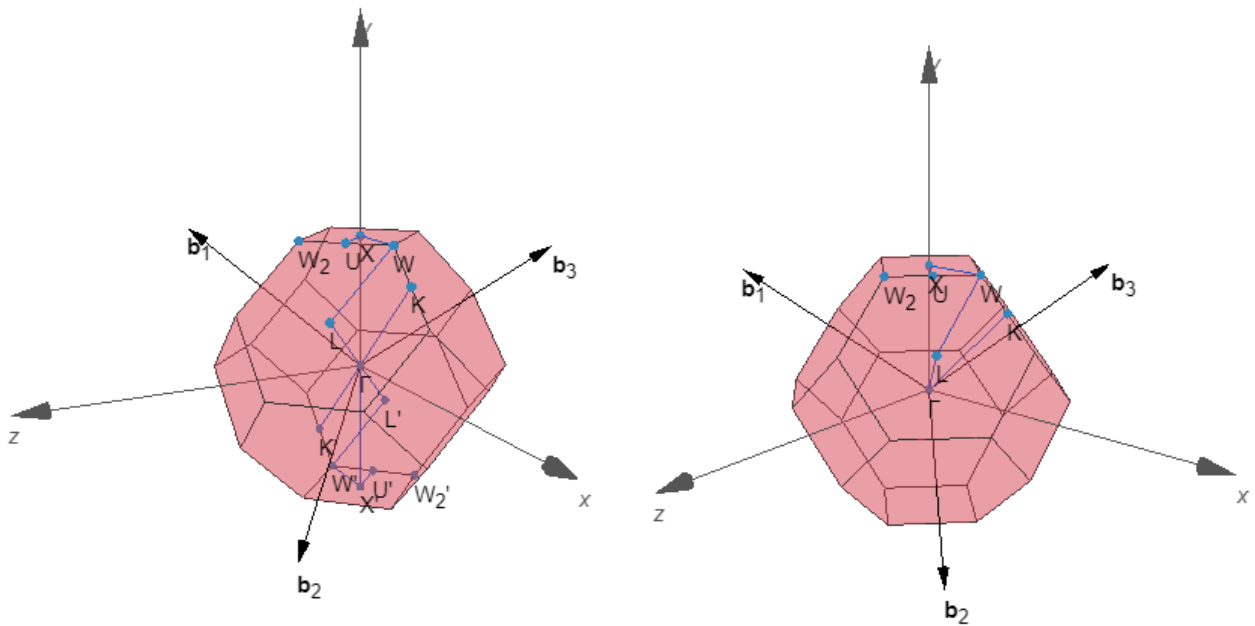
(a) First Brillouin zone for Zincblende phase.   (b) First Brillouin zone for Rocksalt phase.

Figure 13: The first Brillouin zone made with the reference [18]

In Figures 13 and 14 we can see the representation of the first Brillouin zone for the different phases that we had in the zinc sulfide. The Brillouin zones and the band structures are related to each other by the Bloch Theorem:

- **Bloch Theorem**: We can write a complete set of eigenstates, $\Psi_{n\mathbf{k}}(\mathbf{r}) = e^{i\mathbf{k}\cdot\mathbf{r}}u_{n\mathbf{k}}(\mathbf{r})$, for

ideal crystals with a lattice periodic Hamilton satisfying $\hat{H}(\mathbf{r}+\mathbf{R}) = \hat{H}(\mathbf{r})$ for all vectors $\mathbf{R}$ of the Bravais lattice. The associeted energies $E_n(\mathbf{k})$ are continuous functions in the Bloch vector $\mathbf{k}$, which are restricted to the first Brillouin zone for each band index n and constitute the energy bands. [19, 20]
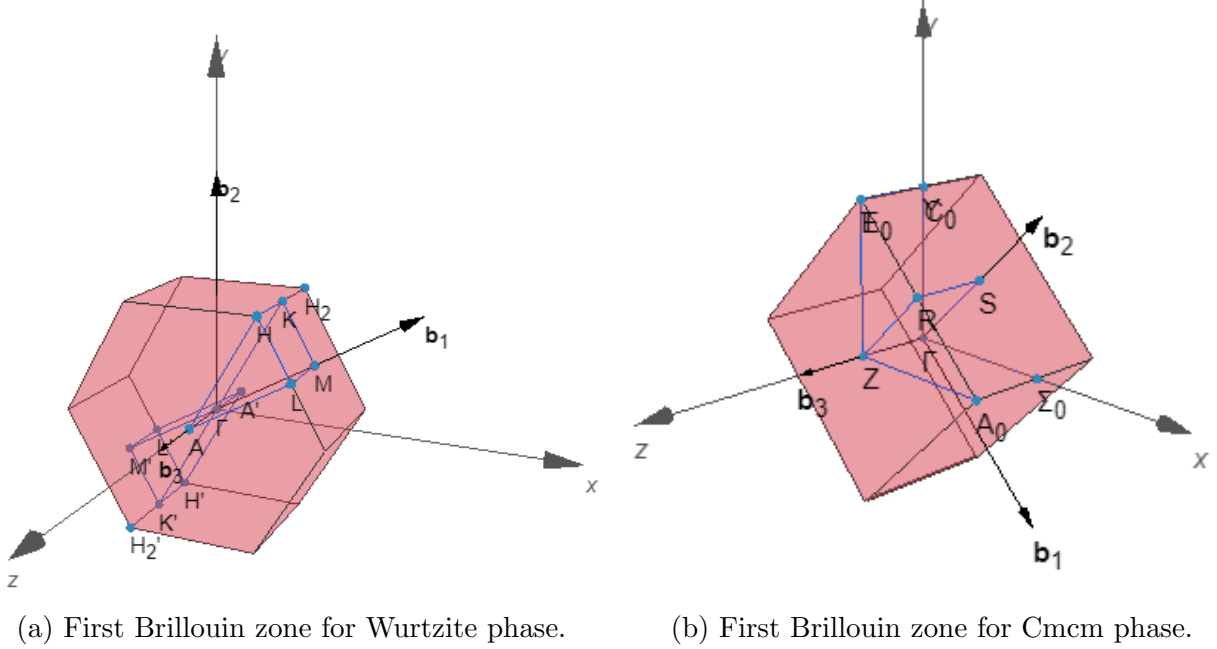

(a) First Brillouin zone for Wurtzite phase.   (b) First Brillouin zone for Cmcm phase.

Figure 14: The first Brillouin zone made with the reference [18]

We can now start with the representations of the different band structures obtained with the program VASP and the correspondign density of states for each of them. As it can be appreciated, we made a study in different volume to see how the compression could affect to the band structure of a material. For the Zincblende and the Rocksalt we used the same K-path because, as it can be observed, their Brillouin zone is almost the same, for Wurtzite and Cmcm phases we used different K-path that where obtained as I mentioned before.

As we were expecting in accordance with the bibliography, the phase represented in Figure 15 presents a semiconducting behavior. It can be seen that all the bands get closer to each other as we increase the volume, this behavior can also be noticed in the bandgaps that we have put together in the Table 3. The density of states is represented in the right side of the graphics, named DOS.

| Volume $35.5[\mathring{A}^3]$	Volume $40.5[\mathring{A}^3]$	Volume $45.5[\mathring{A}^3]$
$2.60[eV]$	$2.01[eV]$	$1.53[eV]$

Table 3: Bandgaps for Zincblende.
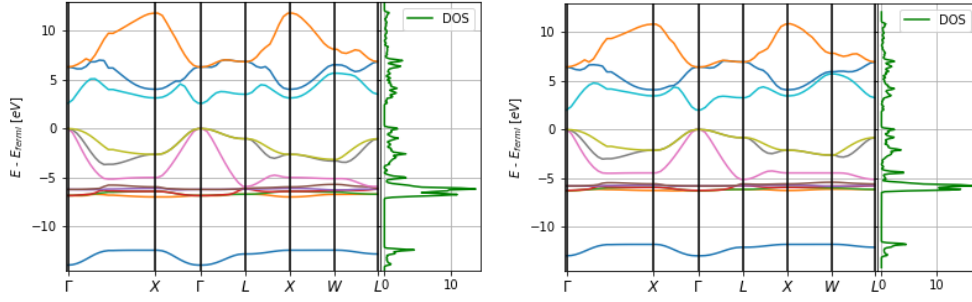
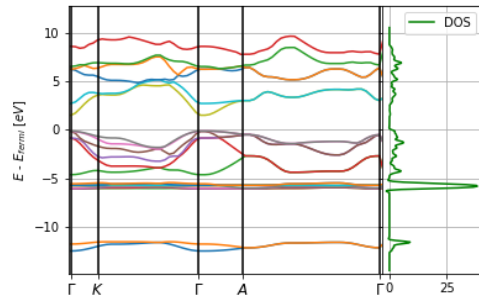(a) For a volume of 35.5 $[\dot{A}^3]$. per atom (b) For a volume of 40.5 $[\dot{A}^3]$ per atom.
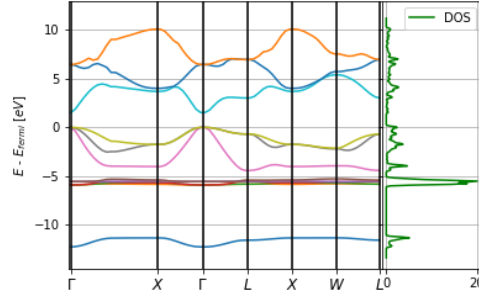
(c) For a volume of 45.5 $[\dot{A}^3]$ per atom.

Figure 15: Bandgaps for Zincblende at different compressions.

The next phase under study is Wurtzite, that can be observed in Figure 16. In this case we also have a semiconducting phase that changes with the pressure at the same rate of Zincblende, as seen in Table 4. This is an interesting feature considering the their band structure, or their Brillouin zone, does not look similar to Zincblende.
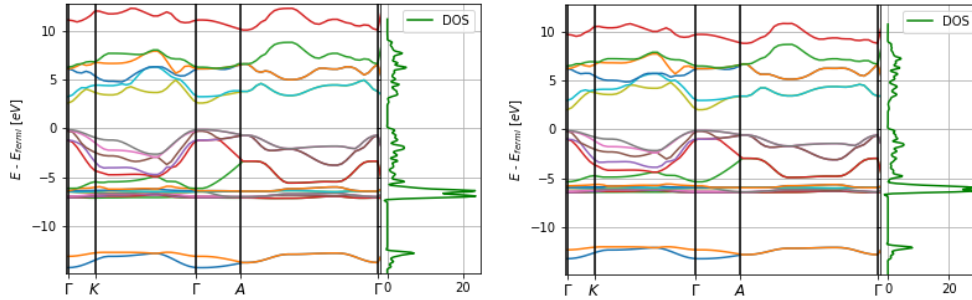
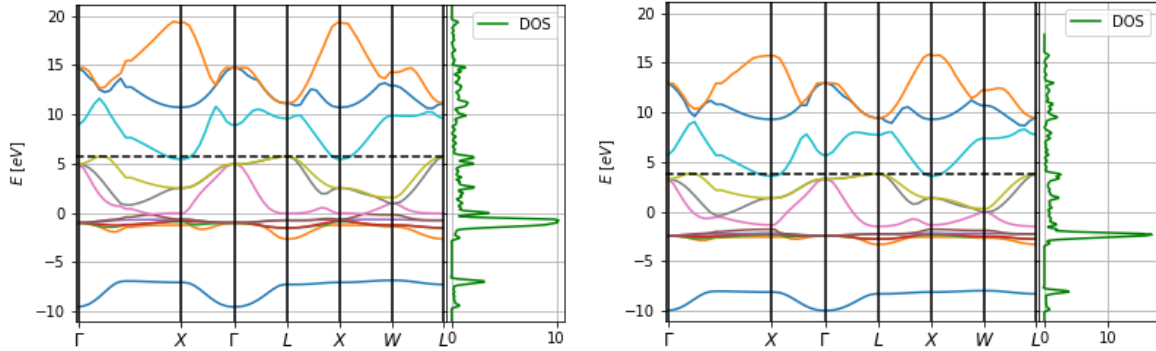(a) For a volume of 35 $[\dot{A}^3]$ per atom. (b) For a volume of 40 $[\dot{A}^3]$ per atom.

(c) For a volume of 45 $[\dot{A}^3]$ per atom.

Figure 16: Bandgaps for Wurtzite at different compressions.

| Volume 35[$\dot{A}^3$]	Volume 40[$\dot{A}^3$]	Volume 45[$\dot{A}^3$]
2.72[eV]	2.13[eV]	1.63[eV]

Table 4: Bandgaps for Wurtzite.

In this part we will get into the study of Rocksalt and Cmcm phases, we can also call them high pressure phases because, as que have seen before, they only appear in this material whe it is at that pressure. We can deduce from the information represented in the graphic that both of them are metallic phases, and that they also present a certain behaviour with the pressure, as we observed in Zincblende and Wurtzite.

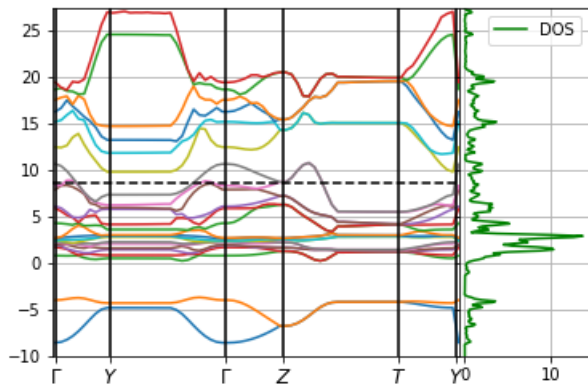(a) For a volume of 28 [$\dot{A}^3$] per atom.
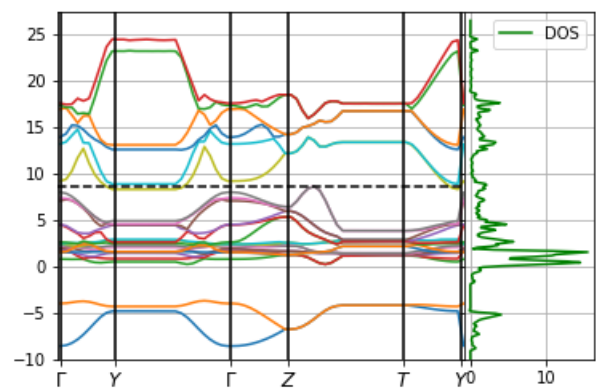
(b) For a volume of 33 [$\dot{A}^3$] per atom.
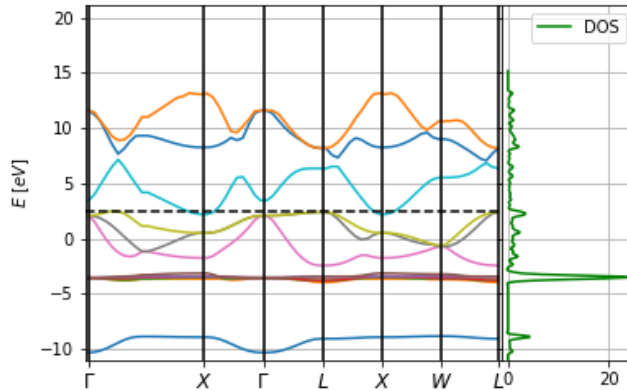
(c) For a volume of 38 [$\dot{A}^3$] per atom.

Figure 17: Bandgaps for the Rocksalt at different compressions.

We will like to highly the different in energies that all the phase represent. For Zincblende and Wurtzite the maximum energy was below $15eV$ while for the other phases, Cmcm and NaCl, that number was higher than 20. It seems that the maximum energy in the band structure increase when we increase the applied pressure.

(a) For a volume of 20 $[\dot{A}^3]$ per atom.

(b) For a volume of 22.5 $[\dot{A}^3]$ per atom.

Figure 18: Bandgaps for the Cmcm at different compressions.

5   Conclusions

In this work I was introduced to the Density Functional Theory, which allowed me to calculate some microscopic parameters from ab initio quantum theory, and then compare them with the experimental values. I obtained similar results for most of the work that manifest the accuracy of the method. I worked for most of the project with two programs, the VASP, that implemented the DFT and that had to be studied exclusively for this project (which gave me more knowledge in a field that I was not familiar with), and Python, which was used to treat the data and where I had to investigate some new components to be able to use it with more efficacy. The first program was located in a Linux console, so I had to learn the basics of this OS to be able to use it. I also mentioned another program, VESTA, this one was in my computer and, thanks to a course in the university, I knew how to use it.

This work has grant me the opportunity of working with new concepts and see how a real study in science is made, which made me realize the quantity of hours that goes into the first part of any project, the investigation of the concepts and what has already been studied. It has also allowed me to investigate and see the problems that scientists face when they are looking for information for their projects, and to use new tools that are used right now by many physics around the world.

As for the project, it was interesting to discover how many things can change in a material when you compres it. It was quite difficult to find data to compare my data for Cmcm phase with other investigations, the same thing happened with wurtzite phase. I would like to highly the importance of this type of studies that allow us to know more about the possible materials that could be used in computers or engineering.

Bibliography

[1] *PhD Thesis Mújica Fernaud, Andrés: "Estabilidad Estructural Y Polimorfismo En Semi-conductores IVa Y IIIa-Va a Alta Presión." (Universidad de la Laguna, 2000)*

[2] *Parr, Robert G; Weitao, Ynag: "Density-Functional Theory of Atoms and Molecules." (Oxford University Pess, 1989)*

[3] *Differents extracts about the Hohenberg-Kohn Theorem:*
   https://www.sciencedirect.com/topics/engineering/hohenberg-kohn-theorem

[4] *R. M. Dreizler; Eberhard K. U. Gross: "Density Functional Theory." (Springer, 2011)*

[5] *Grosso, Giuseppe; Patori Parravicini, Giuseppe: "Solid State Physics." (Academic Press, 2014)*

[6] *Malvin H. Palos; Paula A. Whitlock: "Monte Carlo methods." (2008)*

[7] *Information given by the cretors of the program VASP:*
   https://www.vasp.at/wiki/index.php/VASP_workshop_2003

[8] *Tutorial of the program VASP:*
   https://www.nersc.gov/assets/Uploads/VASP-tutorial-AtomsMoleculesBulk.pdf

[9] Information about the material under study:
   https://es.wikipedia.org/wiki/Sulfuro_de_cinc

[10] *S. Desgreniers; L. Beaulieu; I. Lepage: "Pressure-induced structural changes in ZnS." (Physical Review B. 61 (13) 2000)*

[11] *Birch, Francis: "Finite Elastic Strain of Cubic Crystals". (Physical Review. 71 (11): 809–824, 1947)*

[12] *López-Solano, J.; A. Mújica, P. Rodríguez-Hernández; A. Muñoz: "Theoretical Study of ZnS under High Pressure." (Physica Status Solidi (b) 235.2: 452-55, 2003)*

[13] *Tool on the internet to find the symmetry:*
   https://stokes.byu.edu/iso/findsym.php

[14] *Tool on the internet that gives the k-points:*
   https://www.cryst.ehu.es/cgi-bin/cryst/programs/nph-wp-list

[15] *Mújica, A.; Angel Rubio; A. Muñoz; R. J Needs: "High-pressure Phases of Group-IV, III–V, and II–VI Compounds." (Reviews of Modern Physics 75.3: 863-912, 2003)*

[16] *A. Qteish; M. Abu-Jafar; A. Nazzal: "The instability of the cinnabar phase of ZnS under high pressure" (J. Physics: Condensed Matter, Vol.10, 1998)*

[17] *Kh. Kabita; B. Indrajit sharma; R. K. Brojen Singh; R. K. Thapa: "Structural properties, phase transition and electronic structure of InP and ZnS compound: Density-functional theory LDA, GGA, mbj-GGA calculations" (IOSR-JAP: Vol 10, Issue 6, 2018)*

[18] *Tool on the internet that gives the k-path and the Brillouin zone:*
https://www.materialscloud.org/work/tools/seekpath

[19] *Wacker, Andreas: "An introduction to the Concept of Band Structure." (Lund University, 2018)*
http://www.matfys.lth.se/staff/Andreas.Wacker/Scripts/bandstructure_intro.pdf

[20] *Some information about Bloch Theorem:*
https://www.ucm.es/data/cont/media/www/pag-17832/Propiedades%20Fisicas_Guiones.pdf